Performance Analysis of Intelligent Reflecting Surface Aided Wireless Networks with Wireless Power Transfer

Faissal El Bouanani, *Senior Member, IEEE,* Sami Muhaidat, *Senior Member, IEEE,*
Paschalis C. Sofotasios, *Senior Member, IEEE,* Octavia A. Dobre, *Fellow, IEEE,* and Osamah Badarneh

***Abstract*—The low efficiency of wireless power transfer (WPT) poses a key challenge for energy-constrained wireless networks. To address this issue, in this letter, the integration of intelligent reflecting surface (IRS) into a WPT network is investigated. Specifically, an accurate approximation for the probability density function of the end-to-end cascaded fading channel is presented. By leveraging the derived result, accurate closed-form expressions of the outage probability (OP) and average symbol error probability (ASER) are derived for the proposed IRS-aided WPT system. To gain further insight into the system performance, asymptotic closed-form expressions for the ASER and OP are further derived and interesting observations are made. Particularly, our asymptotic analysis reveals that the achievable diversity in the underlying scenario is independent of the reflective elements of the IRS. The analytical derivations, corroborated by simulation results, demonstrate that IRSs can be promising candidates to realize a highly efficient power transfer enabled wireless network.**

***Index Terms*—Average symbol error rate (ASER), intelligent reflecting surface (IRS), wireless power transfer (WPT).**

I. Introduction

Intelligent Reflecting Surface (IRS) has recently emerged as a disruptive technology, which is envisioned to revolutionize wireless communications by allowing a full control of the propagation environment. Therefore, IRSs are envisaged to play a key role, particularly in multicell multiple-input multiple-output (MIMO) communication networks [1]-[2]. Furthermore, IRSs can realize significant performance gain while enjoying a notable reduction in energy efficiency [3]. Recently, there have been extensive research efforts on the integration of IRS into wireless networks [4]-[6].

This work was supported in part by the Natural Sciences and Engineering Research Council of Canada (NSERC).

F. El Bouanani is with ENSIAS College of Engineering, Mohammed V University, 10000 Rabat, Morocco (e-mail: faissal.elbouanani@um5.ac.ma).

S. Muhaidat is with the Center for Cyber-Physical Systems, Department of Electrical Engineering and Computer Science, Khalifa University, Abu Dhabi 127788, UAE (e-mail: muhaidat@ieee.org).

P. C. Sofotasios is with the Department of Electrical Engineering and Computer Science, Khalifa University of Science and Technology, Abu Dhabi, UAE, and also with the Department of Electrical Engineering, Tampere University, Tampere, Finland, (e-mail: p.sofotasios@ieee.org).

O. A. Dobre is with the Department of Electrical and Computer Engineering, Memorial University, St. John's, NL A1C 5S7, Canada (e-mail: odobre@mun.ca).

O. S. Badarneh is with the Electrical and Communication Engineering Department, School of Electrical Engineering and Information Technology, German-Jordanian University, Amman 11180, Jordan (e-mail: Osamah.Badarneh@gju.edu.jo).

On the other hand, wireless power transfer (WPT) was proposed as a promising solution to provide perpetual energy replenishment for low power wireless networks [7]-[9]. Recently, IRSs have shown a great ability to beamsteer electromagnetic waves, thus enabling highly efficient power transfer [10]-[11].

Our key contributions in this paper can be summarized as follows. First, we derive an accurate approximation, in terms of the univariate Fox H-function, for the probability density function (PDF) of the end-to-end (e2e) wireless fading channel. Then, we derive closed-form expressions for the PDF of the e2e instantaneous signal-to-noise ratio (SNR), outage probability (OP), and average symbol error rate (ASER). Finally, asymptotic expressions for the OP and ASER are derived. It is further demonstrated that while the considered system performance is improved by increasing the number of REs, the diversity order is always limited to 1.

II. System Model

We consider a wireless system scenario, which consists of a single energy source (ES), an IRS of area $a \times b$ with N REs, where a and b denote the width and height of the IRS, respectively, and two wireless sensor nodes, i.e., S_1 and S_2, as depicted in Fig. 1.

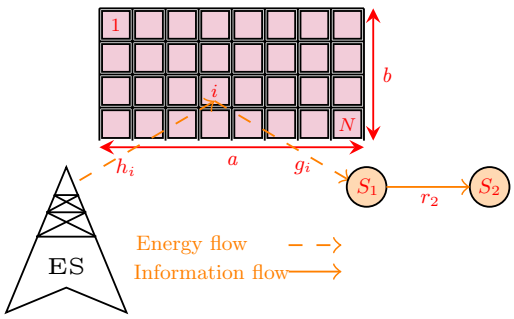

Fig. 1. System setup.

Let us denote the distance between the ES and the IRS by d_0, and that between the IRS and S_1 by d_1. In our setup, we assume all nodes are equipped with a single antenna, and data transmission is performed in two phases as follows:

In phase I, the ES transmits an RF signal to S_1 through the IRS. It is assumed that the transmitted energy of S_1 is limited to the energy harvested from the received ES signal.

By considering the case where the delay spread of the e2e channel is much smaller than the symbol period, the received signal at S_1 can be written as [12, Eq. (23)]

$$y_1 = \sqrt{\beta_1 P_B} \sum_{i=1}^{N} h_i g_i \alpha_i e^{j\theta_i} x_B + n_1, \tag{1}$$

where $\beta_1 = G_{\text{ES}} G_{\text{S}_1}^{(r)} \left(\frac{ab\cos(\theta_{\text{in}})}{4\pi N d_0 d_1} \right)^2$, with G_{ES} and $G_{\text{S}_1}^{(r)}$ as the gain of the ES and receive antenna at S_1, respectively, and θ_{in} as the incident angle from ES to IRS, which is assumed to be equal to the observation angle (i.e., ideal case). Further, h_i and g_i denote the fading coefficients of ES-RE$_i$ and RE$_i$-S_1, respectively. The channel gains are assumed to be independent and identically distributed (i.i.d) and circularly symmetric complex Gaussian (CSCG) distributed with zero mean and identical variance σ^2, i.e., $h_i, g_i \sim \mathcal{CN}(0, \sigma^2)$. Furthermore, P_B denotes the power of the transmitted RF signal from the ES, while $n_1 \sim \mathcal{CN}(0, N_0)$, with N_0 as the noise power spectral density at S_1. At the IRS, $\phi_i = \alpha_i \exp(j\theta_i)$ denotes the response of the RE$_i$, where α_i is the amplitude reflection coefficient and θ_i is the phase shift induced by the RE$_i$ element. For simplicity, both h_i and g_i are assumed to be perfectly known and compensated at the IRS, i.e., $\theta_i = -(\theta_{h_i} + \theta_{g_i})$, where θ_{h_i} and θ_{g_i} denote the arguments of h_i and g_i, respectively. Also, without loss of generality, we assume that α_i equal to 1. Therefore, the harvested power at S_1 can be expressed as

$$P_e = \eta \beta_1 P_B r_1^2, \tag{2}$$

where $r_1 = \sum_{i=1}^{N} |h_i| |g_i|$ and η accounts for energy conversion efficiency.

In phase II, node S_1 utilizes the harvested power in (2) to send its own signal x_2 to S_2. Thus, the received signal at S_2 can be written taking into account the path loss due to large-scale fading, as

$$y_2 = \sqrt{\beta_2 P_e} r_2 x_2 + n_2 = \sqrt{\eta \beta_1 \beta_2 P_B} r_1 r_2 x_2 + n_2, \tag{3}$$

where $\beta_2 = G_{\text{S}_1}^{(t)} G_{\text{S}_2} \left(\frac{\lambda}{4\pi} \right)^2 \frac{d_{2,\text{ref}}^{\rho-2}}{d_2^{\rho}}$, with G_{S_2} and $G_{\text{S}_1}^{(t)}$ as the gain of S_2 and the transmit antenna at S_1, λ as the wavelength, d_2 as the distance between S_1 and S_2, $d_{2,\text{ref}}$ as the reference distance corresponding to a point located in the far field of S_1, and ρ as the path-loss exponent. Further, r_2 and n_2 denote the fading gain of the second hop and the thermal noise at S_2, respectively, and are assumed to be CSCG distributed, i.e., $r_2 \sim \mathcal{CN}(0, \sigma^2)$ and $n_2 \sim \mathcal{CN}(0, N_0)$.

III. Performance Analysis

In this section, the PDF of the e2e cascaded channel gain $R = r_1 |r_2|$ is derived, and based on it, the OP, ASER, and diversity order of the considered RIS-assisted WPT system are derived.

A. OP and ASER Analysis

In this subsection, accurate approximate expressions for the PDFs of $R = r_1 |r_2|$ and e2e instantaneous SNR, OP, and ASER are derived.

1) PDF of R and e2e instantaneous SNR:

Lemma 1. *The PDF of R can be tightly approximated by*

$$f_R(r) \approx \frac{a_1}{\sqrt{2}\sigma} H_{1,3}^{3,0} \left(\frac{r}{\sqrt{2}\sigma a_2} \middle| \begin{matrix} -; (a_3, 1) \\ \Omega_1; - \end{matrix} \right), \tag{4}$$

where $\Omega_1 = \left\{ \left(\frac{1}{2}, \frac{1}{2}\right), (a_4, 1), (a_5, 1) \right\}$, $H_{\cdot,\cdot}^{\cdot,\cdot}[.|.]$ denotes the Fox's H-function [14, Eq. (1.1.1)], $\Gamma(\cdot)$ represents the Gamma function [13, Eq. (6.1.1)], a_i, μ_3, and μ_4 are given by (5)-(7)*, as shown at the top of next page, $\varphi_i = \mu_i / \mu_{i-1}$, with $\mu_0 = 1$, $\mu_1 = N\pi\sigma^2/2$, and $\mu_2 = \left(4 + (N-1)\pi^2/4\right) N\sigma^4$.*

Proof. The PDF of R can be expressed as

$$f_R(r) = \int_0^{\infty} f_{r_1}\left(\frac{r}{x}\right) f_{|r_2|}(x) \frac{dx}{x}. \tag{8}$$

By using the approximate PDF of the summation of double Rayleigh RVs [15, Eq. (14)] and the PDF of $|r_2|$, which is Rayleigh distributed, one can obtain

$$\begin{aligned} f_R(r) &\approx \frac{a_1}{\sigma^2} \int_0^{\infty} e^{-\frac{x^2}{2\sigma^2}} G_{1,2}^{2,0} \left(\frac{r}{x a_2} \middle| \begin{matrix} -; a_3 \\ a_4, a_5; - \end{matrix} \right) dx \\ &\overset{(a)}{=} \frac{a_1}{\sigma^2 2\pi j} \int_{\mathcal{C}_1} \frac{\Gamma(s+a_4)\Gamma(s+a_5)}{\Gamma(s+a_3)} \left(\frac{r}{a_2}\right)^{-s} \\ &\times \int_0^{\infty} x^s \exp\left(-\frac{x^2}{2\sigma^2}\right) dx ds \\ &\overset{(b)}{=} a_1 \int_{\mathcal{C}_1} \frac{\Gamma(s+a_4)\Gamma(s+a_5)\Gamma\left(\frac{s}{2}+\frac{1}{2}\right)}{\sqrt{2}\sigma 2\pi j \Gamma(s+a_3) \left(\frac{r}{\sqrt{2}\sigma a_2}\right)^s} ds, \end{aligned}$$

where $j^2 = -1$, $\mathcal{C}_1$ is an appropriate vertical complex line of integration ensuring the convergence of the above Mellin-Barnes integral (e.g., $[b_1 - j\infty, b_1 + j\infty]$) with $b_1 > \max(-\mathcal{R}(a_4), -\mathcal{R}(a_5)) = -\mathcal{R}(a_5)$, and $\mathcal{R}(.)$ denotes the real part of a complex number. Moreover, step (a) holds using the Mellin-Barnes form of the Meijer's G-function, while step (b) follows from [13, Eq. (3.381.10)]. This completes the proof of (4). ∎

Lemma 2. *The mean and standard deviation of R are given by $\mu_R = N\left(\frac{\pi\sigma^2}{2}\right)^{\frac{3}{2}}$ and $\sigma_R = \sigma^3 \sqrt{8 + \frac{\pi^2 N}{2}\left[N\left(1 - \frac{\pi}{4}\right) - 1\right]}$, respectively.*

Proof. Let $\mu_1^{(2)}$ denote the mean of $|r_2|$, then the mean and the variance of R can be evaluated as $\mu_R = \mu_1 \mu_1^{(2)}$ and $\sigma_R^2 = 2\sigma^2\mu_2 - \mu_R^2$, respectively. By replacing $\mu_1^{(2)}$ by $\sigma\sqrt{\pi/2}$, the proof of Lemma 2 is concluded. ∎

Based on **Lemma 1**, the PDF of the e2e instantaneous SNR $\gamma = \alpha R^2$, with $\alpha = \eta\beta_1\beta_2\widehat{\gamma}$ and $\widehat{\gamma} = \frac{P_B}{N_0}$ is given by

$$\begin{aligned} f_\gamma(\gamma) &= \frac{1}{2\sqrt{\alpha\gamma}} f_R\left(\sqrt{\frac{\gamma}{\alpha}}\right) \\ &\overset{(a)}{\approx} \frac{a_1}{4\alpha\sigma^2 a_2} H_{1,3}^{3,0} \left(\frac{\sqrt{\gamma}}{\sqrt{2\alpha}\sigma a_2} \middle| \begin{matrix} -; (a_3 - 1, 1) \\ \Omega_2; - \end{matrix} \right), \end{aligned} \tag{9}$$

where $\Omega_2 = \left\{ \left(0, \frac{1}{2}\right), (a_4 - 1, 1), (a_5 - 1, 1) \right\}$, and step (a) follows using [14, Eq. (2.1.5)].

2) OP: OP is defined as the probability that the e2e instantaneous SNR falls below a predefined threshold γ_{th}.

$$a_1=\frac{\Gamma(a_3+1)}{a_2\Gamma(a_4+1)\Gamma(a_5+1)}, a_2=\frac{a_3}{2}\left(\varphi_4-2\varphi_3+\varphi_2\right)+2\varphi_4-3\varphi_3+\varphi_2, a_3=\frac{4\varphi_4-9\varphi_3+6\varphi_2-\mu_1}{-\varphi_4+3\varphi_3-3\varphi_2+\mu_1}, \tag{5}$$

$$a_4=\frac{a_6+a_7}{2}, a_5=\frac{a_6-a_7}{2}, a_6=\frac{a_3\left(\varphi_2-\mu_1\right)+2\varphi_2-\mu_1}{a_2}-3, a_7=\sqrt{\left(a_6+2\right)^2-4\frac{\mu_1(a_3+1)}{a_2}}, \tag{6}$$

$$\mu_3=\begin{cases} N\pi\left[6N-\frac{3}{2}+\frac{(N-1)(N-2)\pi^2}{8}\right]\sigma^6, N\geq 3 \\ 21\pi\sigma^6, N=2 \\ \frac{9\pi\sigma^6}{2}, N=1 \end{cases}, \mu_4=\begin{cases} \left(64N+N(N-1)\left[48+\frac{(N-2)(N-3)\pi^4}{16}+3(2N-1)\pi^2\right]\right)\sigma^8, N\geq 4 \\ \left(480+90\pi^2\right)\sigma^8, N=3 \\ \left(224+18\pi^2\right)\sigma^8, N=2 \\ 64\sigma^8, N=1 \end{cases} \tag{7}$$

$$\begin{aligned}\mathcal{L}\left(\gamma_{th}\right) &\overset{(a)}{=} \frac{1}{2\pi j}\int_{\mathcal{C}_2}\frac{\Gamma\left(t+a_4-1\right)\Gamma\left(t+a_5-1\right)\Gamma\left(\frac{t}{2}\right)}{\Gamma\left(t+a_3-1\right)}\frac{\gamma_{th}^{-\frac{t}{2}+1}\left(\sqrt{2\alpha}\sigma a_2\right)^t}{\left(-\frac{t}{2}+1\right)}dt \\ &\overset{(b)}{=} 4\alpha\sigma^2a_2^2\int_{\mathcal{C}_2}\frac{\Gamma\left(s+a_4+1\right)\Gamma\left(s+a_5+1\right)\Gamma\left(\frac{s}{2}+1\right)\Gamma\left(-s\right)}{2\pi j\Gamma\left(s+a_3+1\right)\Gamma\left(1-s\right)}\left(\frac{1}{\sqrt{2}\sigma a_2}\sqrt{\frac{\gamma_{th}}{\alpha}}\right)^{-s}ds.\end{aligned} \tag{12}$$

Proposition 1. *Given a threshold SNR, OP can be accurately approximated by*

$$P_{out}\approx a_1a_2H_{2,4}^{3,1}\left(\frac{\sqrt{\gamma_{th}}}{\sqrt{2\alpha}\sigma a_2}\middle|\begin{matrix}(1,1);(a_3+1,1)\\ \Omega_3;(0,1)\end{matrix}\right), \tag{10}$$

with $\Omega_3=\left\{\left(1,\frac{1}{2}\right),\left(a_4+1,1\right),\left(a_5+1,1\right)\right\}$.

Proof. For a fixed threshold γ_{th}, the OP can be computed using (9) as

$$P_{out}\approx\frac{a_1}{4\alpha\sigma^2a_2}\mathcal{L}\left(\gamma_{th}\right), \tag{11}$$

where $\mathcal{L}\left(.\right)$ is expressed in (12) at the top of the page; equality (a) holds using the Mellin-Barnes representation of the Fox's H-function in (9), while identity (b) follows relying on [13, Eq. (8.331.1)] and using a change of variable $s=t-2$. Substituting (12) into (11), yields (10). Furthermore, since the top left pole of the above integrand is $b_2=\max(-\mathcal{R}(a_4-1),-\mathcal{R}(a_5-1),-2)=-2$, and the bottom right one equals 0, $\mathcal{C}_2$ can be taken the vertical line $[-1-j\infty,-1+j\infty]$. This concludes the proof. ∎

3) ASER: The following proposition presents an accurate approximate expression for the ASER of the underlying IRS-assisted WPT system.

Proposition 2. *For various coherent M-ary modulation schemes, the approximate ASER can be expressed as*

$$P_s\approx\frac{\theta a_1a_2}{2\sqrt{\pi}}H_{3,4}^{3,2}\left(\frac{1}{\sqrt{\alpha\delta}\sigma a_2}\middle|\begin{matrix}\Omega_4\\ \Omega_3;(0,1)\end{matrix}\right), \tag{13}$$

where $\Omega_4=\left\{\left(1,1\right),\left(\frac{1}{2},\frac{1}{2}\right);\left(a_3+1,1\right)\right\}$*, and θ and δ are two constants depending on the modulation scheme [16, Table 6.1].*

Proof. The ASER for different M-ary modulations with coherent detection can be expressed as [16]

$$P_s=\theta\int_0^\infty Q\left(\sqrt{\delta\gamma}\right)f_\gamma\left(\gamma\right)d\gamma, \tag{14}$$

where $Q(.)$ denotes the Q-function, while θ and δ depend on the modulation scheme.

Now, substituting (9) into (14), we obtain (15) given at the top of next page, where the equality (a) holds using integration by part, the derivative of Q-function [16, Eq. (6.42)], and noting that $Q(0)=\frac{1}{2},Q(\infty)=0$, while step (b) follows from [13, Eq. (8.331.1)]. Besides, as the top left and bottom right poles of the above integrand are the same as those of $\mathcal{C}_2$, it follows that $\mathcal{C}_3=\mathcal{C}_2$. Hence, (13) is obtained. ∎

B. Asymptotic Analysis and Diversity Order

Since P_{out} and P_s are expressed in terms of the Fox's H-function or equivalently the Mellin-Barnes integrals, it can be shown that both integrands in (12) and (15) have exactly three different left poles of first-order which depend on a_4 and a_5, as detailed in the proof of Proposition 3. Consequently, a_4 and a_5 lower bounds will determine the asymptotic expressions of both the OP and ASER as illustrated next.

Lemma 3. *For $N>3$, a_4 and a_5 in (6) are real-valued numbers with $a_4>a_5>1$.*

Proof. First, note that μ_i and φ_i are proportional to σ^{2i} and σ^2, respectively. It follows from (5) that a_3 is independent of σ^2 while a_2 depends on σ. As a result, one can determine from (6) that $\left(a_i\right)_{i\geq 4}$ depends on N, and a_7 is a real positive for $N>3$. It follows that a_4 and a_5 are real-valued numbers and $a_4>a_5$.

Fig. 2 shows $\log\left(a_5\right)$ for various values of N. It is clearly seen that such function is positive and increasing on N. Consequently, one can conclude that $a_5>1$. ∎

By using **Lemma 3**, P_{out} and P_s can be asymptotically approximated by only one residue of the integrands in (12) and (15), which corresponds to the top left poles.

Proposition 3. *In the high SNR regime, OP and ASER can be asymptotically approximated as*

$$P_{out}\sim\frac{a_1\Gamma\left(a_4-1\right)\Gamma\left(a_5-1\right)\gamma_{th}}{2\sigma^2\eta\beta_1\beta_2a_2\Gamma\left(a_3-1\right)\widehat{\gamma}}, \tag{16}$$

$$P_s\sim\frac{a_1\Gamma\left(a_4-1\right)\Gamma\left(a_5-1\right)\theta}{4\sigma^2\eta\beta_1\beta_2a_2\Gamma\left(a_3-1\right)\delta\widehat{\gamma}}. \tag{17}$$

$$P_s \overset{(a)}{=} \theta \left\{ \underbrace{\lim_{x\to+\infty} \left[Q\left(\sqrt{\delta\gamma}\right) F_\gamma(\gamma) \right]_0^x}_{=0} + \frac{\sqrt{\delta}}{2\sqrt{2\pi}} \int_0^\infty \frac{1}{\sqrt{\gamma}} e^{-\frac{\delta\gamma}{2}} F_\gamma(\gamma)\, d\gamma \right\}$$
$$\overset{(b)}{\approx} \frac{\theta a_1 a_2}{2\sqrt{\pi}} \frac{1}{2\pi j} \int_{\mathcal{C}_3} \frac{\Gamma(s+a_4+1)\,\Gamma(s+a_5+1)\,\Gamma\left(\frac{s}{2}+1\right)\Gamma\left(\frac{-s}{2}+\frac{1}{2}\right)\Gamma(-s)}{\Gamma(s+a_3+1)\,\Gamma(1-s)} \left(\frac{1}{\sqrt{\alpha\delta}\sigma a_2}\right)^{-s} ds. \tag{15}$$

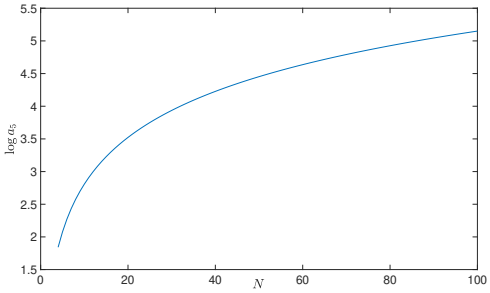

Fig. 2. The function $\log a_5$ for various values of the number of REs.

Remark 1. *It is clear from* (16) *and* (17) *that the maximum achievable diversity order is* $d_v = 1$.

Proof. At high SNR (i.e., $\widehat{\gamma} \to \infty, \alpha \to \infty$), it is clear that the Mellin-Barnes integral in (12) can be written as the infinite summation of residues computed at the left poles (i.e., $-a_4 - 1 - \ell, -a_5 - 1 - \ell, -2 - 2\ell$, with $\ell \in \mathbb{N}$) [14]. It follows that the asymptotic expression of OP can be evaluated as the minimum of the three aforementioned residues computed for $\ell = 0$, namely

$$P_{out} \sim a_1 a_2 \min\left[\mathcal{I}_1, \mathcal{I}_2(a_4, a_5), \mathcal{I}_2(a_5, a_4)\right], \tag{18}$$

where

$$\mathcal{I}_1 = \frac{\Gamma(a_4 - 1)\,\Gamma(a_5 - 1)\,\gamma_{th}}{2\alpha\sigma^2 a_2^2 \Gamma(a_3 - 1)}, \tag{19}$$

and

$$\mathcal{I}_2(x,y) = \frac{\Gamma(x-y)\,\Gamma\left(\frac{-y+1}{2}\right)\Gamma(y+1)}{\Gamma(a_3 - y)\,\Gamma(y+2)} \left(\frac{\gamma_{th}}{2\alpha\sigma^2 a_2^2}\right)^{\frac{y+1}{2}}. \tag{20}$$

Using **Lemma 3**, one obtains $P_{out} \sim a_1 a_2 \mathcal{I}_1$. Finally, by replacing α with $\eta\beta_1\beta_2\widehat{\gamma}$, we obtain (16).

On the other hand, as the left poles of the integrand in (12) and (15) are the same, following similar steps as in the asymptotic expression of ASER can be evaluated as

$$P_s \sim \frac{\theta a_1 a_2}{2\sqrt{\pi}} \min\left[\mathcal{J}_1, \mathcal{J}_2(a_4, a_5), \mathcal{J}_2(a_5, a_4)\right], \tag{21}$$

where

$$\mathcal{J}_1 = \frac{\sqrt{\pi}\Gamma(a_4 - 1)\,\Gamma(a_5 - 1)}{2\Gamma(a_3 - 1)\left(\sqrt{\alpha\delta}\sigma a_2\right)^2}, \tag{22}$$

and

$$\mathcal{J}_2(x,y) = \frac{\Gamma(x-y)\,\Gamma\left(\frac{-y+1}{2}\right)\Gamma\left(\frac{y+2}{2}\right)\Gamma(y+1)}{\Gamma(a_3 - y)\,\Gamma(y+2)\left(\sqrt{\alpha\delta}\sigma a_2\right)^{y+1}}. \tag{23}$$

Again, by leveraging **Lemma 3**, the diversity order can be obtained as $d_v = \min\left[1, \frac{a_4+1}{2}, \frac{a_5+1}{2}\right] = 1$, and the asymptotic ASER is $P_s \sim \frac{\theta a_1 a_2}{2\sqrt{\pi}} \mathcal{J}_1$. Finally, substituting $\alpha = \eta\beta_1\beta_2\widehat{\gamma}$ into (22), we obtain (17). ■

IV. Numerical and Simulation Results

In this section, we investigate the performance of the proposed IRS-aided WPT scheme in terms of OP and ASER. The simulation is performed by generating $3N \times 10^7$ random samples and setting $\sigma^2 = 1, G_{\text{ES}} = G_{\text{S}_1}^{(r)} = G_{\text{S}_1}^{(t)} = G_{\text{S}_2} = 21$ dB, $\lambda = 28.6$ mm, $a \times b/N = 10^{-4}$ m^2, $\theta_{\text{in}} = \pi/6, d_0 = d_1 = d_2 = d_{2,\text{ref}} = 100$ m, and $\rho = 2.2$, i.e., $\beta_1 = 2.5091 \times 10^{-15}$ and $\beta_2 = 8.2094 \times 10^{-6}$.

Fig. 3 depicts the approximate PDF of R for different N values. It can be seen that the proposed approximation is tight for all values of N, validating the accuracy of (9). Furthermore, it can be deduced from Fig. 3 that as N increases, both μ_R and σ_R^2, given in **Lemma 2**, increase and the distribution becomes more positively skewed, leading to a better outage performance.

In Fig. 4, we demonstrate the tightness of the derived OP given by (10) for high values of N while fixing the values of η and $\hat{\gamma}$. It can be seen that for a higher number of reflective elements in the IRS, OP is reduced, leading to a significant performance enhancement in the system. This is due to the fact that the greater N is, the greater R is, and the smaller the cumulative distribution function becomes.

Fig. 5 depicts the OP performance versus $\hat{\gamma}$, for different values of N. It can be seen that there is a perfect match between the approximate and asymptotic outage expressions given by (10) and (16), respectively, even for low-medium SNR values. This stems from the fact that the greater N is, the greater a_2 is, and hence, the less the argument of the Fox's H-function in (10) becomes, making its approximation by only one residue, as shown in (11), sufficiently accurate. Furthermore, it can be straightforwardly noticed that the OP decreases as N increases and/or as the SNR threshold decreases. It is also observed that the diversity order, d_v, is limited to one and independent of N. Note that d_v can be evaluated numerically by choosing any two points $\left(\widehat{\gamma}^{(i)}, P_{out}^{(i)}\right), i = 1, 2$, on the performance curve, where $P_{out}^{(i)} \propto \left(\widehat{\gamma}^{(i)}\right)^{-d_v}$ and $d_v = -\log\left(P_{out}^{(2)}/P_{out}^{(1)}\right) / \log\left(\widehat{\gamma}^{(2)}/\widehat{\gamma}^{(1)}\right)$. For instance, one can check that for $N = 2000$ and $\gamma_{\text{th}} = -125$ dBm and by considering any two points on the curve, e.g., $\left(0 \text{ dB}, 7.945 \times 10^{-4}\right)$ and $\left(5 \text{ dB}, 2.513 \times 10^{-4}\right)$, the diversity order is ≈ 1, which confirms our analytical observation in (16).

Fig. 6 presents the approximate, exact, and asymptotic ASER versus average SNR, given by (13), (14), and (17), respectively, for binary frequency-shift keying (BFSK) modulation scheme $(\theta = 1, \delta = 1)$, quadrature phase-shift

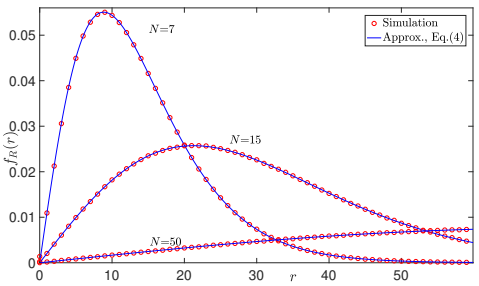

Fig. 3. PDF of R for various values of N.

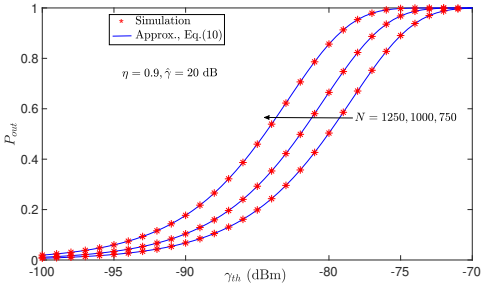

Fig. 4. OP of the considered system.

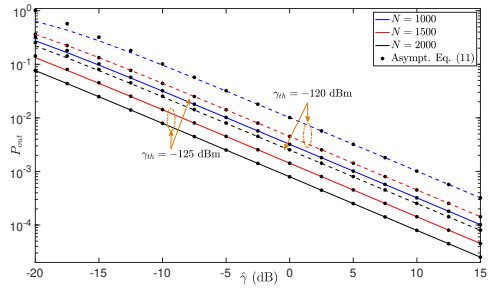

Fig. 5. OP for different values of N and γ_{th}, and $\eta = 0.97$.

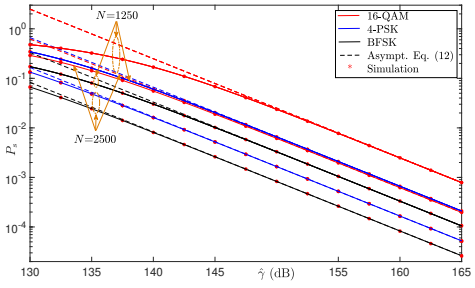

Fig. 6. ASER for various modulations and $\eta = 0.95$.

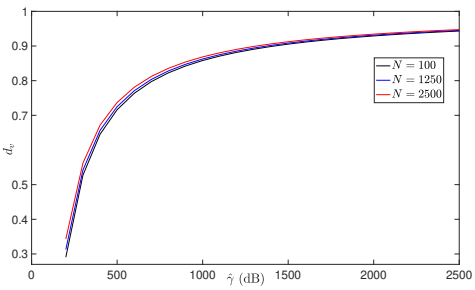

Fig. 7. Asymptotic d_v for 32-QAM and $\eta = 0.97$.

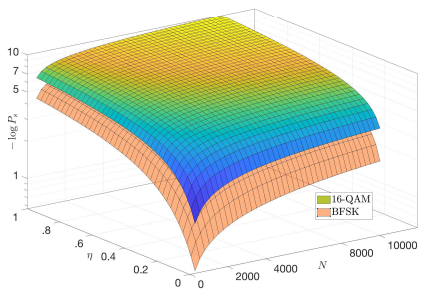

Fig. 8. Logarithm of ASER for $\hat{\gamma} = 150$ dB.

key (QPSK) $(\theta = 2, \delta = 1)$, and 16-ary quadrature amplitude modulation (QAM) $(\theta = 3/2, \delta = 1/5)$ [16, Table 6.1]. It is clearly seen that there is a noticeable improvement in performance as the number of reflective elements increases. Furthermore, it is seen that all curves experience the same diversity order/slope (in logarithmic base 10 scale). It is worth noting that $d_v = 1$.In Fig. 7, the asymptotic d_v is computed by evaluating $-\log P_s / \log \hat{\gamma}$, where P_s is given by (13), as $\hat{\gamma}$ approaches infinity, for 32-QAM $\left(\theta = 2 - \sqrt{2}/4, \delta = 3/31\right)$. Again, it is noticed that d_v approaches unity as $\hat{\gamma}$ increases, and becomes independent of N, confirming our observation in Proposition 3.

Fig. 8 shows the logarithm of inverse ASER as a function of both N and η, for two modulation schemes and $\hat{\gamma} = 150$ dB, evaluated based on (13). It is noticed from (17) that ASER increases with θ/δ and is inversely proportional with η. Thus, BFSK outperforms 16-QAM as $\theta/\delta = 1, 15/2$ for both schemes. It can be further noticed that the ASER performance enhances by increasing both N and η.

V. Conclusion

A new highly accurate expression for the PDF of the e2e cascaded fading channel was presented for an IRS-assisted WPT system. Based on the derived result, closed-form and asymptotic expressions for the OP and ASER were derived. It was shown that while there is a significant improvement in the performance as N increases, the achievable diversity order of the considered system is independent of the number of REs and always limited to one. It was further shown that simulation and analytical results are perfectly matched, validating our approximations and confirming our analytical observations.

References

[1] Q. Wu and R. Zhang, "Intelligent reflecting surface enhanced wireless network: Joint active and passive beamforming design," in *Proc. GLOBECOM*, Dec. 2018, pp. 1-6.

[2] C. Pan et al., "Multicell MIMO communications relying on intelligent reflecting surfaces," *IEEE Trans. Wirel. Commun.*, vol. 19, no. 8, pp. 5218-5233, Aug. 2020.

[3] M. Di Renzo et al., "Smart radio environments empowered by reconfigurable AI meta-surfaces: an idea whose time has come," *EURASIP Journal on Wireless Commun. and Netw.*, no. 1, pp. 1-20, Dec. 2019.

[4] Y. Han, W. Tang, S. Jin, C. Wen, and X. Ma, "Large intelligent surface-assisted wireless communication exploiting statistical CSI," *IEEE Trans. Veh. Technol.*, vol. 68, no. 8, pp. 8238-8242, Aug. 2019.

[5] Q. Wu and R. Zhang, "Intelligent reflecting surface-enhanced wireless network via joint active and passive beamforming," *IEEE Trans. Wireless Commun.*, vol. 18, no. 11, pp. 5394-5409, Nov. 2019.

[6] H. Shen et al., "Secrecy rate maximization for intelligent reflecting surface assisted multi-antenna communications," *IEEE Commun. Lett.*, vol. 23, no. 9, pp. 1488-1492, Sept. 2019.

[7] L. Mohjazi, S. Muhaidat, M. Dianati, and M. Al-Qutayri, "Performance analysis of SWIPT relay networks with noncoherent modulation," *IEEE Trans. Green Commun. and Netw.*, vol. 2, no. 4, pp. 1072-1086, Dec. 2018

[8] L. Mohjazi, S. Muhaidat, M. Dianati and M. Al-Qutayri, and N. Al-Dhahir, "Performance analysis of SWIPT relaying systems in the presence of impulsive noise," *IEEE Access*, vol. 6, pp. 71662-71677, Dec. 2018.

[9] Q. Wu and R. Zhang, "Joint active and passive beamforming pptimization for intelligent reflecting surface assisted SWIPT under QoS constraints," *IEEE J. Sel. Areas Commun.*, vol. 38, no. 8, pp. 5394-5409, Aug. 2020.

[10] C. Pan et al., "Intelligent reflecting surface aided MIMO broadcasting for simultaneous wireless information and power transfer", [Online] Available: https://arxiv.org/pdf/1908.04863.pdf

[11] Q. Wu and R. Zhang, "Weighted sum power maximization for intelligent reflecting surface aided SWIPT," [Online]. Available: https://arxiv.org/abs/1907.05558

[12] Ö. Özdogan, E. Björnson, and E. G. Larsson, "Intelligent reflecting surfaces: Physics, propagation, and pathloss modeling," *IEEE Wireless Commun. Letters*, vol. 9, no. 5, pp. 106-112, Jan. 2020.

[13] I. S. Gradshteyn and I. M. Ryzhik, *Table of Integrals, Series, and Products*, Seventh Edition. Burlington, MA: Elsevier, 2007.

[14] A. Kilbas, *H-Transforms: Theory and Applications*, Analytical Methods and Special Functions, Taylor and Francis, 2004.

[15] L. Bariah, S. Muhaidat, P. C. Sofotasios, F. El Bouanani, O. Dobre, and W. Hamouda, "Large intelligent surfaces-based non-orthogonal multiple access: Performance analysis," submitted to *IEEE Internet Things J.*, May 2020.

[16] A. Goldsmith, *Wireless Communications*. Cambridge Univ. Press, 2005.